FIRST-ORDER PHASE TRANSITION IN THE FRAMEWORK OF THE CELL FLUID MODEL: REGIONS OF CHEMICAL POTENTIAL VARIATION AND THE CORRESPONDING DENSITIES

I.V. PYLYUK[1], M.P. KOZLOVSKII

Institute for Condensed Matter Physics
of the National Academy of Sciences of Ukraine,
1 Svientsitskii Str., 79011 Lviv, Ukraine

A microscopic description is given for the behavior of the fluid system in an immediate vicinity of its critical point, where theoretical and experimental researches are difficult to carry out. For the temperatures $T < T_c$, the regions of chemical potential and density variations are singled out and analyzed. The equation of state of the cell fluid model in terms of temperature-chemical potential is written using the Heaviside functions. This equation is also given in terms of the temperature and density variables. As a result of the study of the relationship between the density and the chemical potential, an equation for the binodal curve is obtained in a narrow neighborhood of the critical point.

1 Introduction

The theoretical and experimental study of the behavior of liquids and their mixtures in a vicinity of their critical point (see, e.g., works [1–8]) is an important and challenging task. In our previous works [9, 10], the behavior of fluid was studied in an immediate vicinity of the critical point, and in works [11–13] beyond this vicinity. As a result, a wide region near the critical point has been covered. The mathematical description was carried out in the framework of the cell fluid model using the grand canonical ensemble. The whole volume V of a system consisting of N interacting particles was

---

[1]e-mail: piv@icmp.lviv.ua

conventionally divided into N_v cells, each of the volume $v = V/N_v = c^3$, where c is the linear cell size. Note that unlike the lattice gas model where the cell is assumed to contain no more than one particle, in this approach the cell can include more than one particle.

In works [9, 10], the analysis was performed in the framework of the collective-variables approach using the renormalization group transformation [14]. An analytical procedure for calculating the grand partition function and the thermodynamic potential of the cell fluid model was developed in works [9,10] in the approximation of a non-Gaussian (quartic) distribution for order parameter fluctuations without involving the hard-spheres reference system. The formation of the reference system as a part of the repulsive component of the interaction potential made it possible to take into account all kinds of interaction (both short- and long-range) from the same position of the collective-variables approach.

The role of interaction potential in this work is played by the Morse potential. The interaction potential parameters, which are given in works [9, 10] and are necessary for quantitative estimates, correspond to the data for sodium. They were taken from work [15], which was devoted to the study of vapor-liquid equilibrium curves for metals using Monte Carlo simulation and Morse potential. Taking this potential into account, the vapor-liquid coexistence curves for metals were also analyzed in the framework of the integral-equations approach [16].

The Morse potential is widely used when studying the melting and laser ablation processes using computer simulation [17–19]. There are works in the literature devoted to the study of the structural properties of the Morse and Lennard-Jones clusters, as well as to a comparison between them [19–22]. In some cases, modifications of the Morse function were made [23–26] in order to improve the numerical results. Although the Morse potential was traditionally used to model covalently bound diatomic molecules [27–29], it is also applied to estimate non-bounding interactions [30, 31]. This potential is qualitatively similar to the Lennard-Jones potential, but they are quite different from the quantitative point of view. The Lennard- Jones and Morse potentials can be compared directly using a mathematical relationship enabling the point of energy minimum to be located at the same position [32,33]. In addition, it was shown that either of the potentials can be derived from the other [34].

This work complements the study of the critical behavior of the Morse fluid that was performed in works [9, 10]. In particular, for temperatures

lower than the critical one, solutions of a certain cubic equation are obtained. They govern the quantities entering the equation of state of the cell fluid model. The behavior of the equation solutions depending on the chemical potential value is analyzed in the immediate vicinity of the critical point, and the regions where the chemical potential changes are singled out. Each of those regions is considered separately. Expressions for the boundary densities (the densities at the regions' boundaries) are obtained. For this purpose, a nonlinear equation, which relates the density to the chemical potential, is used. The equation of state of the cell fluid model and the binodal equation are presented.

2 Chemical potential and density changes at temperatures below the critical one

The equation of state of the cell fluid model for temperatures $T < T_c$ [10] contains quantities dependent on the solution σ'_0 of the equation

$$(\sigma'_0)^3 + p'\sigma'_0 + q' = 0. \tag{1}$$

(the solution is also given in work [10]). The coefficients

$$p' = 6\frac{r_{n'_p+2}}{u_{n'_p+2}}, \quad q' = -6\frac{s^{5/2}}{u_{n'_p+2}}\frac{\tilde{h}}{(\tilde{h}^2 + h_{cm}^2)^{1/2}}$$

include the quantities $r_{n'_p+2}$ and $u_{n'_p+2}$ determining the long-wavelength part of the grand partition function of the model. The quantity $\tilde{h}$ is proportional to the chemical potential M, and the quantity h_{cm} is characterized by the renormalized relative temperature $\tau = (T - T_c)/T_c$ (see work [10]). The renormalization group parameter s determines the separation of the phase space of collective variables into layers.

The form of the solutions of Eq. (1) depends on the sign of the discriminant

$$Q = (p'/3)^3 + (q'/2)^2. \tag{2}$$

If $Q > 0$, the single real solution σ'_0 of Eq. (1), according to Cardano's formula, looks like

$$\begin{aligned}
\sigma'_{0b} &= A + B, \\
A &= (-q'/2 + Q^{1/2})^{1/3}, \\
B &= (-q'/2 - Q^{1/2})^{1/3}.
\end{aligned} \tag{3}$$

3

If $Q < 0$, there are three real solutions (the quantity σ'_0 acquires three possible real values)

$$\sigma'_{01} = 2(-p'/3)^{1/2} \cos(\alpha_r/3),$$
$$\sigma'_{02,03} = -2(-p'/3)^{1/2} \cos(\alpha_r/3 \pm \pi/3), \tag{4}$$

where α_r is determined from the equation

$$\cos \alpha_r = -\frac{q'}{2(-p'/3)^{3/2}}. \tag{5}$$

If the discriminant is negative, solutions (4) can be rewritten as follows:

$$\sigma'_{01} = 2\sigma_{0r} \cos \frac{\alpha_r}{3}, \quad \sigma'_{02} = -2\sigma_{0r} \cos \left(\frac{\alpha_r}{3} + \frac{\pi}{3} \right),$$
$$\sigma'_{03} = -2\sigma_{0r} \cos \left(\frac{\alpha_r}{3} - \frac{\pi}{3} \right). \tag{6}$$

Here,

$$\sigma_{0r} = \left(-\frac{2r_{n'_p+2}}{u_{n'_p+2}} \right)^{1/2},$$
$$\alpha_r = \arccos \left(\frac{M \left(\tilde{h}_q^2 + h_{cm}^2 \right)^{1/2}}{M_q \left(\tilde{h}^2 + h_{cm}^2 \right)^{1/2}} \right). \tag{7}$$

The chemical potential M_q is determined from the condition $Q = 0$ and satisfies the equality

$$M_q = \left[-\frac{8r_{n'_p+2}^3(1 + \alpha_{mq}^2)}{9u_{n'_p+2}s^5\beta W(0)} \right]^{1/2} h_{cm}, \tag{8}$$

where
$$\alpha_{mq} = \tilde{h}_q/h_{cm}, \quad \tilde{h}_q = M_q \left(\beta W(0) \right)^{1/2}. \tag{9}$$

Here, $\beta = 1/(kT)$ is the inverse temperature, and $W(0)$ is the Fourier transform of the effective interaction potential [9] at the zero wave vector. For all $|M| < M_q$, the discriminant $Q < 0$ and, therefore, there are three real roots of Eq. (1) in this interval of M-values.
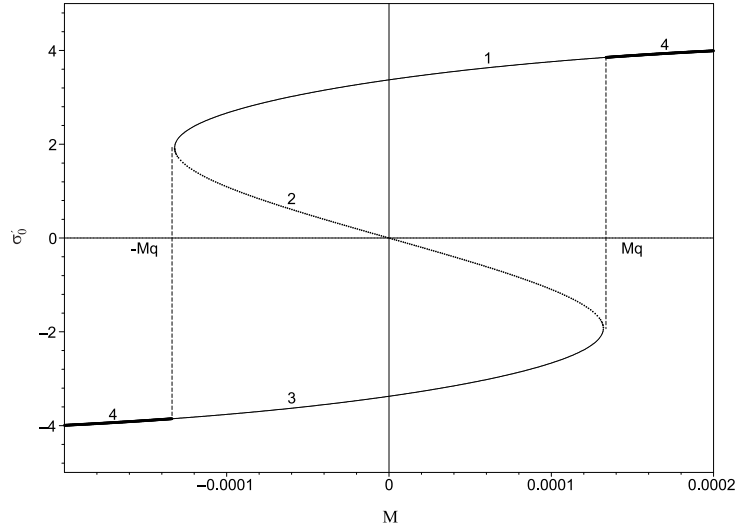
4

Figure 1: Solutions of cubic equation (1) as functions of the chemical potential M at $\tau = -0.005$. Curves 1, 2, 3, and 4 correspond to $\sigma_0' = \sigma_{01}'$, $\sigma_0' = \sigma_{02}'$, $\sigma_0' = \sigma_{03}'$, and $\sigma_0' = \sigma_{0b}'$, respectively.
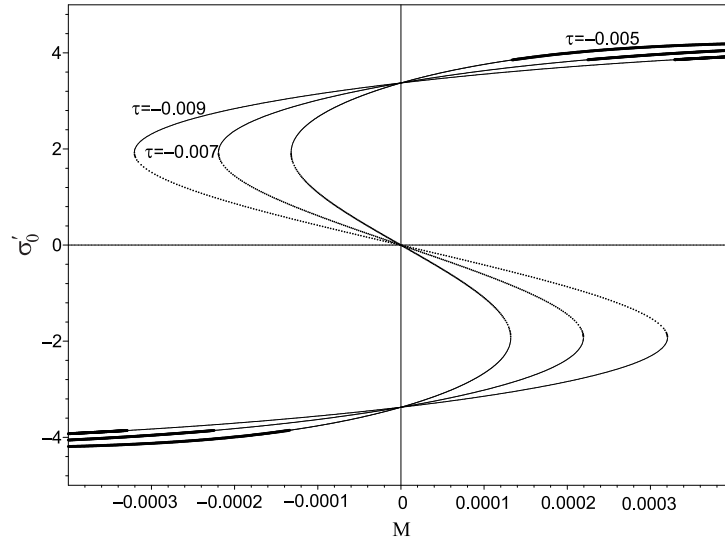

Figure 2: Dependence of the solutions of cubic equation (1) on the chemical potential M at various values of the relative temperature ($\tau = -0.005$, $\tau = -0.007$, $\tau = -0.009$).

5

The dependence of the solutions of the cubic equation (1) on the chemical potential M at $T < T_c$ is shown in Figs. 1 and 2. Figure 2 makes it possible to trace the shift of M_q (the joint points of the thin and thick solid curves) as τ changes. As one can see, the absolute value of M_q decreases with the reduction of $|\tau|$.

In the case $|M| > M_q$, as was at $T > T_c$, Eq. (1) has a single real solution (3). For the latter, at $M = -M_q$ and taking into account the equality $Q = 0$, we obtain

$$\sigma_{0bq}^{'(-)} = 2\left[-3s^{5/2}\frac{M_q(\beta W(0))^{1/2}}{u_{n_p'+2}h_{cm}(1+\alpha_{mq}^2)^{1/2}}\right]^{1/3} = -2\sigma_{0r}, \qquad (10)$$

whereas at $M = M_q$ we have

$$\sigma_{0bq}^{'(+)} = 2\left[3s^{5/2}\frac{M_q(\beta W(0))^{1/2}}{u_{n_p'+2}h_{cm}(1+\alpha_{mq}^2)^{1/2}}\right]^{1/3} = 2\sigma_{0r}. \qquad (11)$$

Let us analyze the asymptotics of solutions (6) at $|M| = M_q$. If $M = -M_q$, we obtain $\cos\alpha_{rq}^{(-)} = -1$, $\alpha_{rq}^{(-)} = \pi$, and

$$\sigma_{01}^{'(-)} = 2\sigma_{0r}\cos\frac{\pi}{3} = \sigma_{0r},$$

$$\sigma_{02}^{'(-)} = -2\sigma_{0r}\cos\left(\frac{2\pi}{3}\right) = \sigma_{0r},$$

$$\sigma_{03}^{'(-)} = -2\sigma_{0r}\cos 0 = -2\sigma_{0r}. \qquad (12)$$

The case $M = M_q$ brings us to the formulas $\cos\alpha_{rq}^{(+)} = 1$, $\alpha_{rq}^{(+)} = 0$, and

$$\sigma_{01}^{'(+)} = 2\sigma_{0r}\cos 0 = 2\sigma_{0r},$$

$$\sigma_{02}^{'(+)} = -2\sigma_{0r}\cos\frac{\pi}{3} = -\sigma_{0r},$$

$$\sigma_{03}^{'(+)} = -2\sigma_{0r}\cos\left(-\frac{\pi}{3}\right) = -\sigma_{0r}. \qquad (13)$$

Thus, if $M = -M_q$, the solution is $\sigma_{0bq}^{'(-)} = -2\sigma_{0r}$ (see Eq. (10)), which coincides with $\sigma_{03}^{'(-)}$ from Eq. (12). If $M = M_q$, the solution is $\sigma_{0bq}^{'(+)} = 2\sigma_{0r}$ (see Eq. (11)) and it coincides with $\sigma_{01}^{'(+)}$ from Eq. (13).
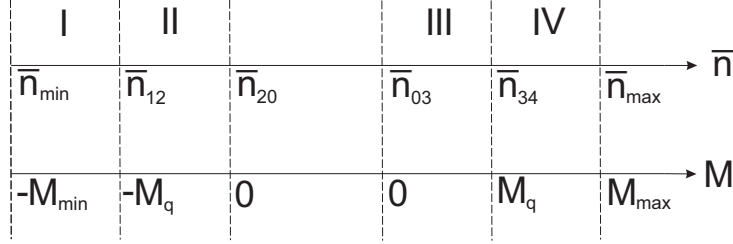
Figure 3: Regions of chemical potential variation and the corresponding densities for temperatures below the critical one.

The conclusion drawn from the above calculations is as follows. As the chemical potential increases to $-M_q$ from the side of negative values, Eq. (1) has a single solution given by Eq. (3) (region I, gas phase, in Fig. 3). At $-M_q < M < 0$, it transforms into the solution σ'_{03} from Eq. (6), which is valid up to $M = -0$ (region II, transient gas phase). For $M = -M_q$, we obtain $\sigma'_{03} = \sigma'^{(-)}_{03} = -2\sigma_{0r}$ (see Eq. (12)), and for $M = -0$, we arrive at the expressions $\cos\alpha^{(-)}_{r0} = 0$, $\alpha^{(-)}_{r0} = \pi/2$, and

$$\lim_{M \to -0} \sigma'_{03} = \sigma'^{(-)}_{030} = -2\sigma_{0r}\cos\left(-\frac{\pi}{6}\right) = -\sqrt{3}\sigma_{0r}. \tag{14}$$

On the other hand, as M decreases to M_q from the side of positive values, there is the single solution (3) (region IV, fluid phase). At $0 < M < M_q$, this solution transforms into the solution σ'_{01} from Eq. (6), which is valid up to $M = +0$ (region III, transient fluid phase). For $M = M_q$, we have $\sigma'_{01} = \sigma'^{(+)}_{01} = 2\sigma_{0r}$ (see Eq. (13)), and for $M = +0$ we obtain

$$\lim_{M \to +0} \sigma'_{01} = \sigma'^{(+)}_{010} = 2\sigma_{0r}\cos\left(\frac{\pi}{6}\right) = \sqrt{3}\sigma_{0r}. \tag{15}$$

According to the chemical potential value M, the equation of state of the cell fluid model at $T < T_c$ (see work [10]) can be written in the form

$$\begin{aligned}
\frac{Pv}{kT} &= P^{(-)}_a(T) + E_\mu + D_{13}(\sigma'_{0b})\left[\Theta(-M - M_q)+\right.\\
&\left.+\Theta(M - M_q)\right] + D_{13}(\sigma'_{03})\Theta(-M)\Theta(M + M_q) +\\
&+D_{13}(\sigma'_{01})\Theta(M)\Theta(M_q - M).
\end{aligned} \tag{16}$$

7

Here, the quantity

$$D_{13}(\sigma'_0) = \left(\gamma_s^{(-)} - e_2^{(-)}\right)\left(\tilde{h}^2 + h_{cm}^2\right)^{\frac{d}{d+2}} +$$
$$+ e_0^{(-)}\tilde{h}\left(\tilde{h}^2 + h_{cm}^2\right)^{\frac{d-2}{2(d+2)}} \tag{17}$$

depends on the solution σ'_0 of Eq. (1); $d = 3$ is the space dimension; v is the cell volume; $\Theta(M)$ is the Heaviside function, which is equal to unity if $M > 0$, to zero if $M < 0$, and to $1/2$ if $M = 0$; the quantity $P_a^{(-)}(T)$ depends analytically on the temperature; the coefficient $\gamma_s^{(-)}$ characterizes the non-analytical contribution to the thermodynamic potential; the quantities $e_0^{(-)}$ and $e_2^{(-)}$ depend on the roots of the cubic equation (1). Expressions for all those quantities, as well as for E_μ, are given in work [10].

The equation of state (16) makes it possible to study the dependence of the pressure P on the chemical potential M and the relative temperature τ. This equation can be rewritten in terms of the temperature and density variables. For this purpose, the chemical potential expressed via the temperature τ and the average density $\bar{n}$ should be substituted into Eq. (16), and the intervals of chemical potential values in the Heaviside functions have to be replaced by the corresponding density values from the regions shown in Fig. 3. Let us consider each of the regions separately.

Region I ($M \leq -M_q$). Here the solution σ'_0 of Eq. (1) looks like σ'_{0b} from Eq. (3). If $M = -M_q$, then expression (10), where σ_{0r} is given by the relationship from Eq. (7), is valid for σ'_{0b}. Solution (10) for $\sigma'^{(-)}_{0bq}$ coincides with $\sigma'^{(-)}_{03}$ from Eq. (12). On the other hand, the equality [10]

$$b_3^{(-)} M^{1/5} = \bar{n} - n_g + M, \tag{18}$$

holds, which couples the average density $\bar{n}$ with the chemical potential (in this case, $M = -M_q$) and the quantity $\sigma_{00}^{(-)} = f(\sigma'_{0b})$, which is included into the coefficient $b_3^{(-)}$. Note that n_g is determined via the coefficients in the initial expression for the grand partition function, and $\sigma_{00}^{(-)}$ is a function of the quantity $\alpha_m = \tilde{h}/h_{cm}$, which includes the initial chemical potential μ (included into M) and the relative temperature τ. From Eq. (18), we can determine the density $\bar{n}_{12}$ (the boundary density between regions I and II) corresponding to the value $M = -M_q$. Neglecting the last term in Eq. (18),

8

we obtain

$$\bar{n}_{12} = n_g + b_3^{(-)} M^{1/5}\big|_{M=-M_q} = n_g + \left[(1+\alpha_{mq}^2)^{1/2} h_{cm}\right]^{1/5} \sigma_{00}^{(-)}(\sigma_{03}^{'(-)}),$$
$$\sigma_{03}^{'(-)} = -2\sigma_{0r}. \tag{19}$$

Region II $(-M_q < M \le -0)$. At $M = -0$, the equality (14) holds true and the boundary density $\bar{n}_{20} = \lim_{M\to-0} \bar{n}$ takes the form

$$\bar{n}_{20} = n_g + \lim_{M\to-0} \left[(1+\alpha_m^2)^{1/2} h_{cm}\right]^{1/5} \sigma_{00}^{(-)} = n_g + h_{cm}^{1/5}\sigma_{00}^{(-)}(\sigma_{030}^{'(-)}),$$
$$\sigma_{030}^{'(-)} = -\sqrt{3}\sigma_{0r}. \tag{20}$$

Region III $(+0 \le M < M_q)$. This region starts from the value $M = +0$, where $\sigma_{010}^{'(+)} = \sqrt{3}\sigma_{0r}$ and, accordingly,

$$\bar{n}_{03} = n_g + h_{cm}^{1/5}\sigma_{00}^{(-)}(\sigma_{010}^{'(+)}). \tag{21}$$

The chemical potential M in region III acquires values less than M_q.

Region IV $(M \ge M_q)$. This region starts from the value $M = M_q$, which corresponds to $\sigma_{01}^{'(+)} = 2\sigma_{0r}$, so that

$$\bar{n}_{34} = n_g + \left[(1+\alpha_{mq}^2)^{1/2} h_{cm}\right]^{1/5} \sigma_{00}^{(-)}(\sigma_{01}^{'(+)}). \tag{22}$$

The initial boundary density $\bar{n}_{34}$ in region IV increases to a certain value $\bar{n}_{max}$, which corresponds to M_{max}. At $\bar{n} > \bar{n}_{max}$, the chemical potential M decreases with the increasing density $\bar{n}$, which does not reflect the physical nature of the phenomenon (a similar picture is observed at $\bar{n} < \bar{n}_{min}$).

The determination of the boundary densities $\bar{n}_{12}$, $\bar{n}_{20}$, $\bar{n}_{03}$, and $\bar{n}_{34}$ makes it possible to write the equation of state (16) in the form

$$\frac{Pv}{kT} = P_a^{(-)}(T) + E_\mu + D_{13}(\sigma_{0b}') \left[\Theta(\bar{n}_{12} - \bar{n}) + \right.$$
$$+ \Theta(\bar{n} - \bar{n}_{34})] + D_{13}(\sigma_{03}')\Theta(\bar{n} - \bar{n}_{12})\Theta(-\bar{n} + \bar{n}_{20}) +$$
$$+ D_{13}(\sigma_{01}')\Theta(\bar{n} - \bar{n}_{03})\Theta(\bar{n}_{34} - \bar{n}), \tag{23}$$

where

$$D_{13}(\sigma_0') = \left(\frac{\bar{n} - n_g}{\sigma_{00}^{(-)}}\right)^6 \left[e_0^{(-)}\frac{\alpha_m}{(1+\alpha_m^2)^{1/2}} + \gamma_s^{(-)} - e_2^{(-)}\right]. \tag{24}$$

The dependence of the pressure P (see Eq. (23)) on $\bar{n}$ for various τ is shown in Fig. 4.
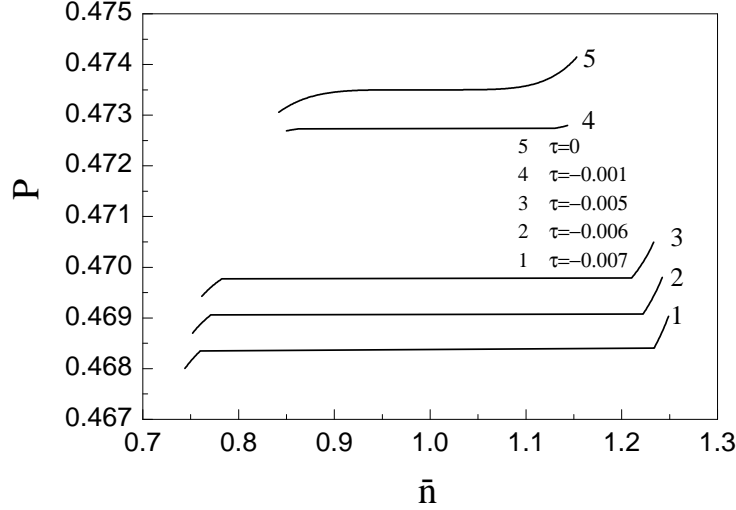
Figure 4: Pressure as a function of average density for various values of the relative temperature.

3 Relationship between the density and the chemical potential of fluid. Limiting cases

Nonlinear equation (18), which describes the relationship between the density $\bar{n}$ and the chemical potential M, can be rewritten in the form [10]

$$\bar{n} = n_g - M + \sigma_{00}^{(-)} \left(\tilde{h}^2 + h_{cm}^2 \right)^{\frac{d-2}{2(d+2)}}. \tag{25}$$

The general form of equation (25) or (18) makes it possible to change in a natural way to the cases when either of the variables (the temperature or the chemical potential) is crucial for the description of the order parameter behavior.

Let us describe the behavior of $\bar{n}$ for some limiting cases. One of them is the absence of chemical potential M (i.e., $M = 0$ and hence $\tilde{h} = 0$) and $T \neq T_c$. Then, we obtain

$$\sigma_{00}^{(-)}(M = 0) = \frac{e_0^{(-)}}{(\beta W(0))^{1/2}} + e_{020}^{(-)}, \tag{26}$$

where

$$e_{020}^{(-)} = e_{02}^{(-)}(M = 0) = \frac{1}{(\beta W(0))^{1/2}} \frac{f_{Iv}}{s^3}.$$

10

The expression for f_{Iv} is given in work [10]. From Eq. (25), we obtain the dependence

$$\bar{n} = n_g + \sigma_{00}^{(-)}(M = 0)\tilde{\tau}_1^\beta, \tag{27}$$

where the critical exponent $\beta = \nu/2$.

Another limiting case is $M \neq 0$ and $T = T_c$. The density $\bar{n}$ in Eq. (25) at $T = T_c$ satisfies the equality

$$\bar{n} = n_g - M + \sigma_{00}^{(-)}(T_c)\tilde{h}^{1/\delta}, \tag{28}$$

where

$$\sigma_{00}^{(-)}(T_c) = \frac{6}{5}\frac{1}{(\beta_c W(0))^{1/2}}\left[e_0^{(-)} + \gamma_s^{(-)} - e_2^{(-)}\right] \tag{29}$$

and the critical exponent $\delta = 5$.

In the general case, i.e., at $M \neq 0$ and $T \neq T_c$, Eq. (25) can be presented as follows:

$$\bar{n} = n_g - M + \sigma_{00}^{(-)}\left(\tilde{h}^2 + \tilde{\tau}_1^{2\beta\delta}\right)^{1/(2\delta)}. \tag{30}$$

Note that $M \ll 1$, and $\tilde{h} \sim M$. Therefore, the second summand, M, in the right-hand sides of Eqs. (25), (28), and (30) is much smaller than the third term and can be neglected.

4   Binodal equation

The binodal equation can be obtained from Eq. (25) by putting $M = 0$. Then we arrive at Eq. (27). Now, substituting the expression $\tilde{\tau}_1 = -\tau\frac{c_{11}}{q}E_2^{n_0}$, we obtain

$$\bar{n} = n_g + \sigma_{00}^{(-)}(M = 0)\left(-\tau\frac{c_{11}}{q}E_2^{n_0}\right)^\beta. \tag{31}$$

Here, E_2 is one of the eigenvalues of the matrix for the linear transformation of the renormalization group, the quantity c_{11} characterizes one of the coefficients in the solutions of recurrence relations for the ρ^4-model [9, 10], n_0 is the difference between the exit points from the critical fluctuation regime at $T > T_c$ and $T < T_c$, and q is associated with the averaging of the wave vector square. For more information on those parameters, see work [10].
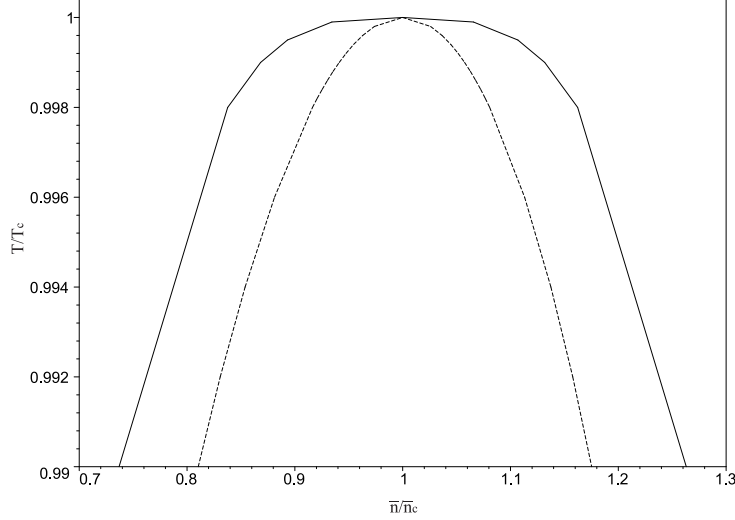
Figure 5: Coexistence curve (binodal curve) obtained in an immediate vicinity of the critical point taking into account the interaction potential parameters that are characteristic of sodium. The solid curve (the dome) was plotted according to the obtained binodal equation, and the dotted curve is a result of the zero-mode approximation [12].

Let us solve Eq. (31) with respect to the temperature. Taking the equalities $\tau = T/T_c - 1$ and $\beta = \nu/2$ into account, we obtain

$$\left[\frac{\left(\frac{\bar{n}}{n_g} - 1 \right) n_g}{\sigma_{00}^{(-)}(M = 0)} \right]^{2/\nu} \frac{q}{c_{11} E_2^{n_0}} = -\frac{T}{T_c} + 1 \tag{32}$$

or

$$\frac{T}{T_c} = 1 - \left\{ \left[\frac{\left(\frac{\bar{n}}{n_g} - 1 \right) n_g}{\sigma_{00}^{(-)}(M = 0)} \right]^2 \right\}^{1/\nu} \frac{q}{c_{11} E_2^{n_0}}. \tag{33}$$

On the basis of Eq. (33), we can plot the binodal curve in the temperature versus density plane (see Fig. 5). This curve agrees with the data predicted for sodium by extrapolating the results of computer simulation [15] to $T/T_c \approx 1$ (see work [10]).

The spinodal equation, which describes the limiting states of the system that determine the boundaries of the instability region, can be found from

the extremum condition

$$\left.\frac{\partial(Pv/kT)}{\partial\bar{n}}\right|_T = 0$$

for the equation of state (23), where we should substitute the chemical potential M expressed from Eq. (18) in terms of the average density $\bar{n}$.

5 Conclusions

In this paper, the cell model was used to study the behavior of fluid in a close vicinity of its critical point. This is an interesting (because of fundamental and applied aspects) and difficult (because of a substantial role of fluctuation effects) issue for analysis. The study of the relationship between the density and the chemical potential at temperatures $T < T_c$ made it possible to determine the corresponding densities in the regions where the chemical potential changes and obtain both the equation of state and the binodal equation. Solutions of a certain cubic equation were presented, which the equation of state of the cell fluid model depends on. Their analysis made it possible to describe the transition from one solution to another when the chemical potential tends to zero. On the basis of the obtained equation of state, the pressure variation with the density growth at various temperatures has been illustrated graphically. Using the binodal equation, a binodal curve in a narrow temperature interval was constructed for the microscopic parameters of the Morse potential that are inherent to sodium. As compared with the case of the zero-mode approximation, the obtained dome of the coexistence curve is wider and agrees better with the results of computer simulation [15].

References

[1] C.-L. Lee, G. Stell, J.S. Høye. A simple SCOZA for simple fluids. *J. Mol. Liq.* **112**, 13 (2004).

[2] C.E. Bertrand, J.F. Nicoll, M.A. Anisimov. Comparison of complete scaling and a field-theoretic treatment of asymmetric fluid criticality. *Phys. Rev. E* **85**, 031131 (2012).

[3] A. Parola, L. Reatto. Recent developments of the hierarchical reference theory of fluids and its relation to the renormalization group. *Mol. Phys.* **110**, 2859 (2012).

[4] I.R. Yukhnovskii. The phase transition of the first order in the critical region of the gas-liquid system. *Condens. Matter Phys.* **17**, 43001 (2014).

[5] T.J. Yoon, Y.-W. Lee. Current theoretical opinions and perspectives on the fundamental description of supercritical fluids. *J. Supercrit. Fluids* **134**, 21 (2018).

[6] L.F. Vega. Perspectives on molecular modeling of supercritical fluids: From equations of state to molecular simulations. Recent advances, remaining challenges and opportunities. *J. Supercrit. Fluids* **134**, 41 (2018).

[7] A. Oleinikova, L. Bulavin, V. Pipich. Critical anomaly of shear viscosity in a mixture with an ionic impurity. *Chem. Phys. Lett.* **278**, 121 (1997).

[8] S. Pittois, B. Van Roie, C. Glorieux, J. Thoen. Thermal conductivity, thermal effusivity, and specific heat capacity near the lower critical point of the binary liquid mixture n-butoxyethanol–water. *J.Chem. Phys.* **121**, 1866 (2004).

[9] M.P. Kozlovskii, I.V. Pylyuk, O.A. Dobush. The equation of state of a cell fluid model in the supercritical region. *Condens. Matter Phys.* **21**, 43502 (2018).

[10] I.V. Pylyuk. Fluid critical behavior at liquid–gas phase transition: Analytic method for microscopic description. *J. Mol. Liq.* **310**, 112933 (2020).

[11] M. Kozlovskii, O. Dobush. Representation of the grand partition function of the cell model: The state equation in the mean-field approximation. *J. Mol. Liq.* **215**, 58 (2016).

[12] M.P. Kozlovskii, O.A. Dobush, I.V. Pylyuk. Using a cell fluid model for the description of a phase transition in simple liquid alkali metals. *Ukr. J. Phys.* **62**, 865 (2017).

[13] I.V. Pylyuk, O.A. Dobush. Equation of state of a cell fluid model with allowance for Gaussian fluctuations of the order parameter. *Ukr. J. Phys.* **65**, 1080 (2020).

[14] I.R. Yukhnovskii. *Phase Transitions of the Second Order. Collective Variables Method* (World Scientific, 1987).

[15] J.K. Singh, J. Adhikari, S.K. Kwak. Vapor–liquid phase coexistence curves for Morse fluids. *Fluid Phase Equilib.* **248**, 1 (2006).

[16] E.M. Apfelbaum. The calculation of vapor-liquid coexistence curve of Morse fluid: Application to iron. *J. Chem. Phys.* **134**, 194506 (2011).

[17] Y. Zhou, M. Karplus, K.D. Ball, R.S. Berry. The distance fluctuation criterion for melting: Comparison of square-well and Morse potential models for clusters and homopolymers. *J. Chem. Phys.* **116**, 2323 (2002).

[18] X. Xu, C. Cheng, I.H. Chowdhury. Molecular dynamics study of phase change mechanisms during femtosecond laser ablation. *J. Heat Transfer* **126**, 727 (2004).

[19] I. Last, Y. Levy, J. Jortner. Beyond the Rayleigh instability limit for multicharged finite systems: From fission to Coulomb explosion. *Proc. Natl. Acad. Sci. USA* **99**, 9107 (2002).

[20] J.P.K. Doye, D.J. Wales. The structure and stability of atomic liquids: From clusters to bulk. *Science* **271**, 484 (1996).

[21] J.P.K. Doye, R.H. Leary, M. Locatelli, F. Schoen. Global optimization of Morse clusters by potential energy transformations. *INFORMS J. Comput.* **16**, 371 (2004).

[22] A. Tekin, M. Yurtsever. Molecular dynamics simulation of phase transitions in binary LJ clusters. *Turk. J. Chem.* **26**, 627 (2002).

[23] C.-I. Chou, C.-L. Ho, B. Hu, H. Lee. Morse-type Frenkel-Kontorova model. *Phys. Rev. E* **57**, 2747 (1998).

[24] A. Strachan, T. Cagin, W.A. Goddard, III. Phase diagram of MgO from density-functional theory and molecular-dynamics simulations. *Phys. Rev. B* **60**, 15084 (1999).

[25] T.-C. Lim. Approximate relationships between the Generalized Morse and the Extended-Rydberg potential energy functions. *Acta Chim. Slov.* **52**, 149 (2005).

[26] A. Del Sol Mesa, C. Quesne, Yu.F. Smirnov. Generalized Morse potential: Symmetry and satellite potentials. *J. Phys. A: Math. Gen.* **31**, 321 (1998).

[27] P.M. Morse, E.C.G. Stueckelberg. Diatomic molecules according to the wave mechanics I: Electronic levels of the hydrogen molecular ion. *Phys. Rev.* **33**, 932 (1929).

[28] A.S. Leal, C. Gouvea dos Santos, C.M. Quintella, H.H.R. Schor. A theoretical model for the scattering of I_2 molecule from a perfluoropolyeter liquid surface. *J. Braz. Chem. Soc.* **10**, 359 (1999).

[29] V. Constantoudis, C.A. Nicolaides. Stabilization and relative phase effects in a dichromatically driven diatomic Morse molecule: Interpretation based on nonlinear classical dynamics. *J. Chem. Phys.* **122**, 084118 (2005).

[30] A.I. Milchev, A.A. Milchev. Wetting behavior of nanodroplets: The limits of Young's rule validity. *Europhys. Lett.* **56**, 695 (2001).

[31] D. Osorio-Gonzalez, M. Mayorga, J. Orozco, L. Romero-Salazar. Entropy and thermalization of particles in liquids. *J. Chem. Phys.* **118**, 6989 (2003).

[32] P. Shah, C. Chakravarty. Instantaneous normal mode analysis of Morse liquids. *J. Chem. Phys.* **116**, 10825 (2002).

[33] H. Okumura, F. Yonezawa. Liquid–vapor coexistence curves of several interatomic model potentials. *J. Chem. Phys.* **113**, 9162 (2000).

[34] T.-C. Lim. The relationship between Lennard-Jones (12-6) and Morse potential functions. *Z. Naturforsch.* **58a**, 615 (2003).